Supplementary material

Lattice-expanded NiSe Catalyst via Lanthanum Incorporation for Accelerating Urea Electrooxidation in Assisting Water Electrolysis

Quan Zhang, Hejin Ma, Ruobing Han, Tonglin Yang, Zhenhui Chen, Miaoyang Zhu,

Jiawei Shi*, Weiwei Cai*, Fangqi Yang*, and Zehui Yang*

Table of Contents

S1. Experimental details.

Computational methods

All first-principles calculations were performed using the Vienna Ab initio Simulation Package (VASP 5.4.4)[1], based on density functional theory (DFT) with plane-wave basis sets and the projector augmented wave (PAW) method[2,3]. The exchange-correlation interactions were treated using the Perdew-Burke-Ernzerhof (PBE) functional[4] within the generalized gradient approximation (GGA). The electronic wave functions were described using plane waves with a kinetic energy cutoff of 450 eV. To account for van der Waals interactions, we incorporated the DFT-D3 dispersion correction scheme with Becke–Johnson damping[5].

To model the NiSe(101) surface, we employed a four-atomic-layer slab with a 15 Å vacuum layer along the surface normal to minimize periodic image interactions. The lanthanum-doped NiSe (La-NiSe) catalyst was constructed by replacing a Ni atom in the topmost layer with La atom. For Brillouin zone integration, a Monkhorst-Pack mesh of $2 \times 2 \times 1$ *k*-points was employed[6]. During geometry optimization, all atoms were allowed to relax except that the lowest two layers of the slab kept the atomic positions as in the bulk metal. Atomic positions were optimized using the conjugate gradient algorithm with a convergence criterion of 0.03 eV/Å for forces on atoms. In all the cases of structural optimization, the energy convergence was set to 1×10^{-5} eV.

The adsorption energy (ΔE_{ads}) of an adsorbate on the NiSe and La-NiSe surfaces is defined as follows:

$$\Delta E_{ads} = E_{adsorbate/surface} - E_{surface} - E_{adsorbate}$$

where $E_{adsorbate/surface}$, $E_{surface}$, and $E_{adsorbate}$ are the total energy of adsorbate and substrate system in the equilibrium state, the energy of bare metal slab, and the energy of free adsorbate, respectively. A more negative adsorption energy is indicative of a higher thermodynamic stability of the adsorption structure.

S2. Structure characterization of catalysts.

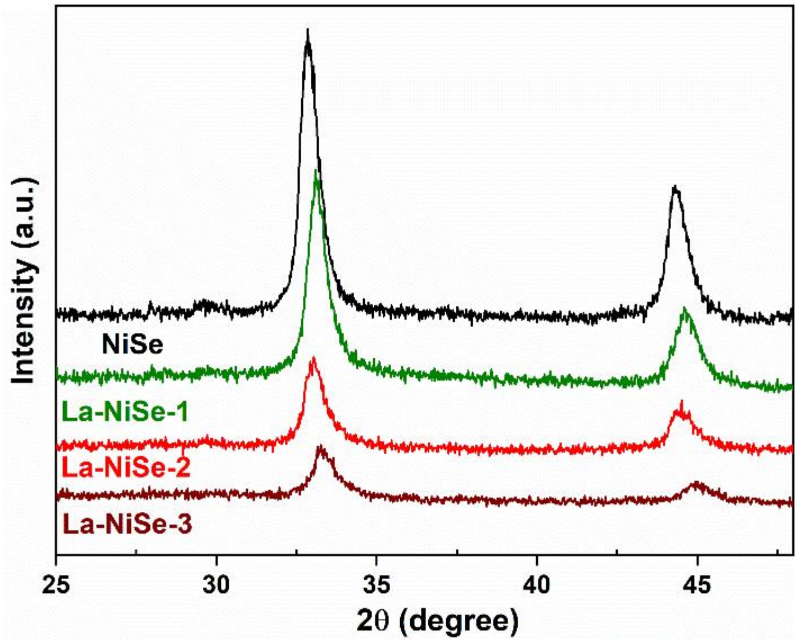

Figure S1. Enlarged XRD patterns of various La-NiSe and NiSe electrocatalysts.

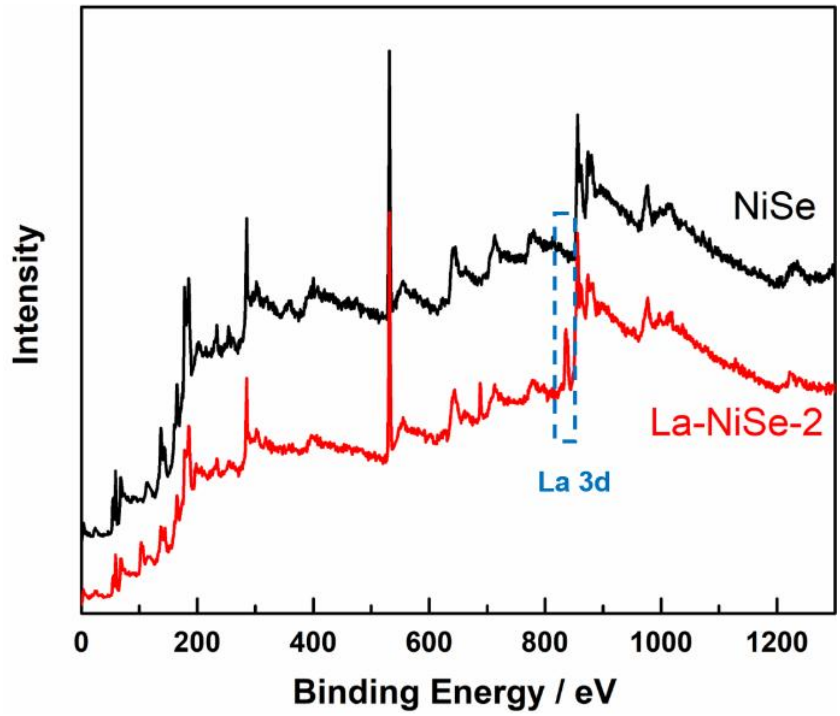

Figure S2. The full-spectrum XPS of the La-NiSe-2 and NiSe electrocatalysts.

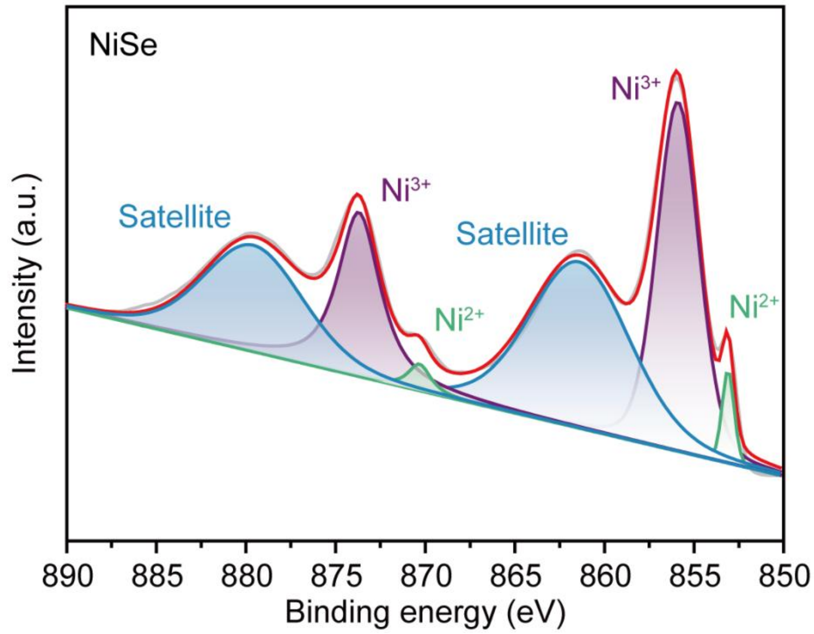

Figure S3. Deconvoluted XPS spectra of Ni 2p of the NiSe.

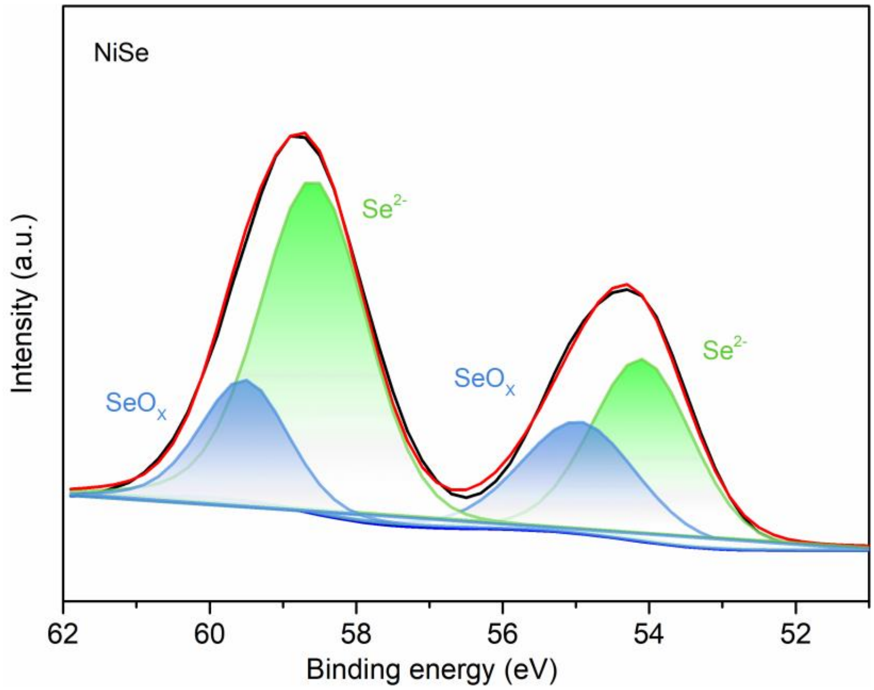

Figure S4. Deconvoluted XPS spectra of Se 3d of NiSe.

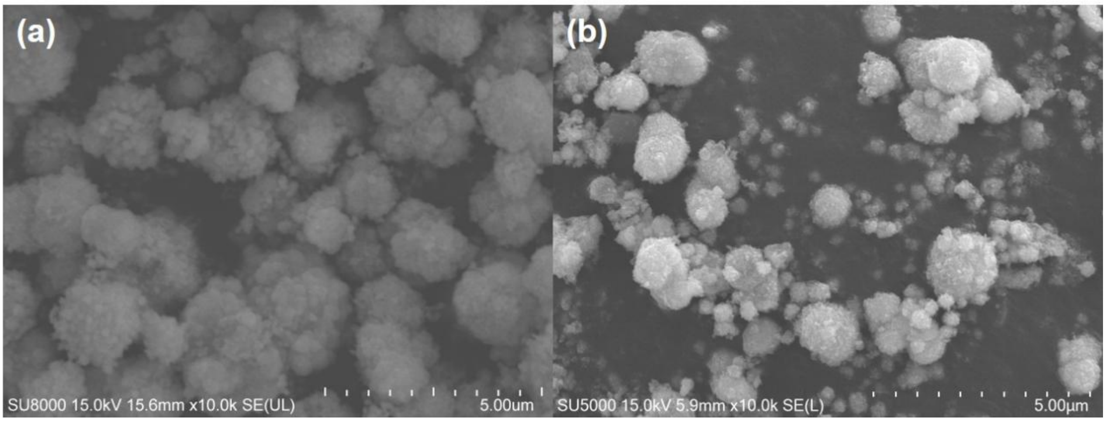

Figure S5. The FESEM of the (a) NiSe and (b) La-NiSe-2 electrocatalysts.

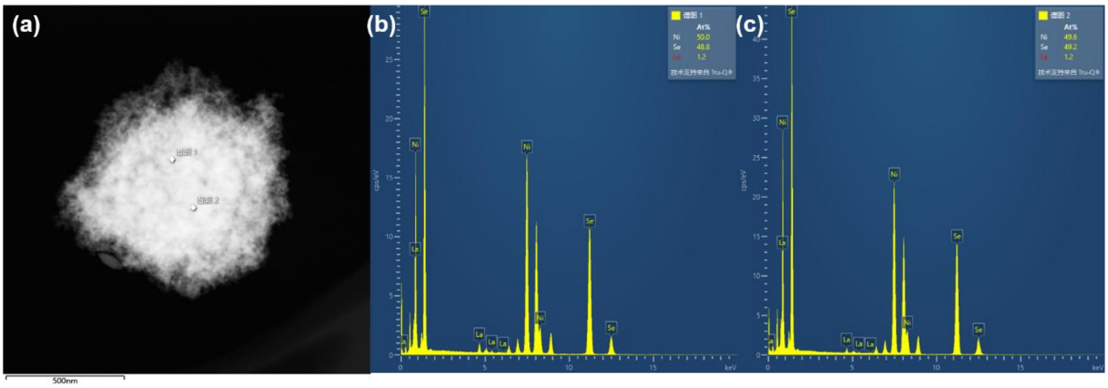

Figure S6. (a) HAADF-STEM image and its EDX point scan analysis images (b,c) of the La-NiSe-2 electrocatalysts.

S3. Electrochemical characterization.

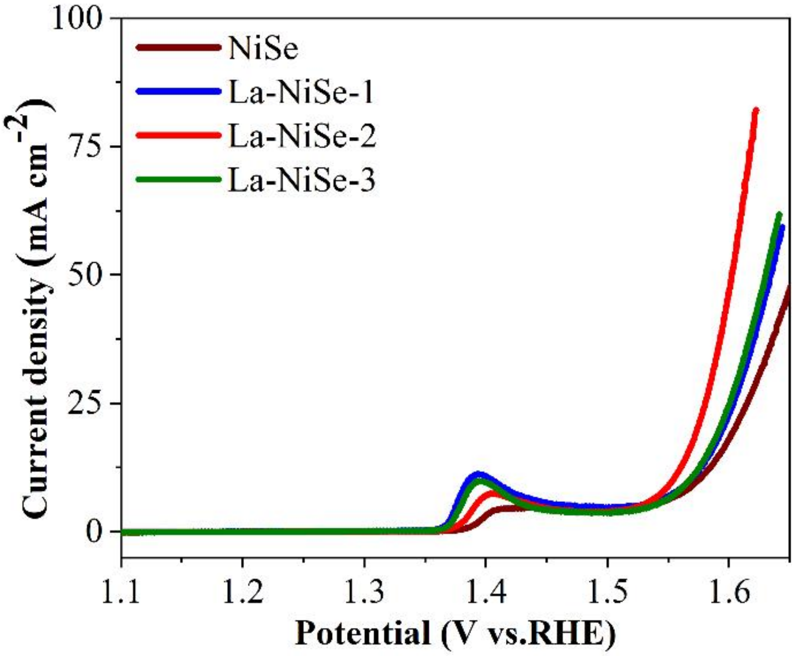

Figure S7. The LSV curves of the various La-NiSe and NiSe electrocatalysts in 1 M KOH electrolyte.

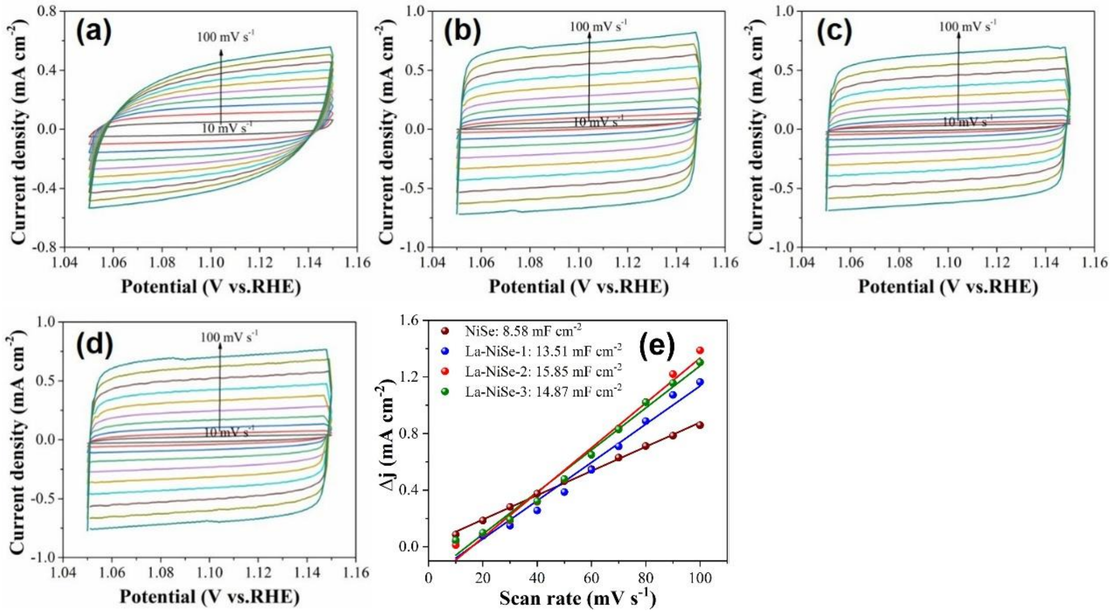

Figure S8. The CV curves of the (a) NiSe, (b) La-NiSe-1, (c) La-NiSe-2, (d) La-NiSe-3 electrocatalysts and corresponding (e) C_{dl} values in 1 M KOH with 0.33 M urea solution.

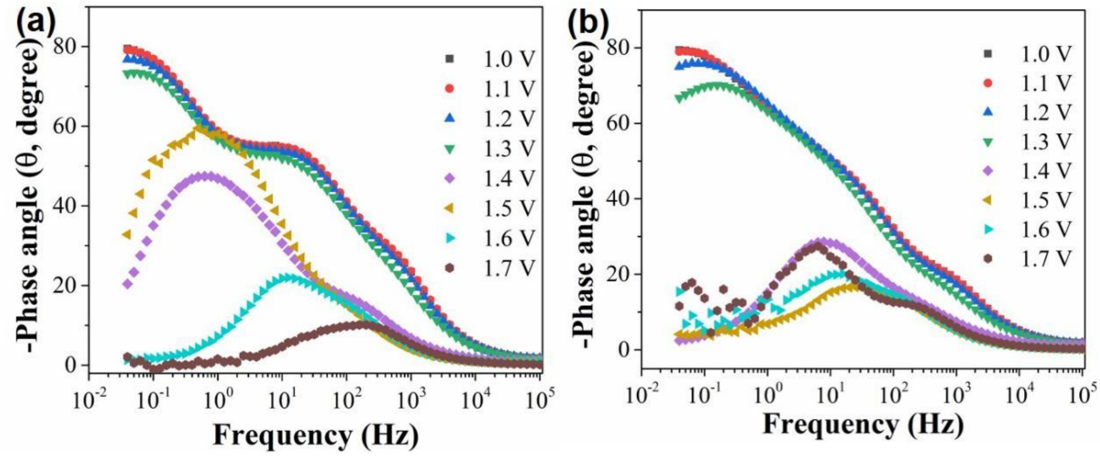

Figure S9. Bode plots of operando EIS of NiSe catalyst in 1 M KOH (a) without and (b) with 0.33 M urea solution.

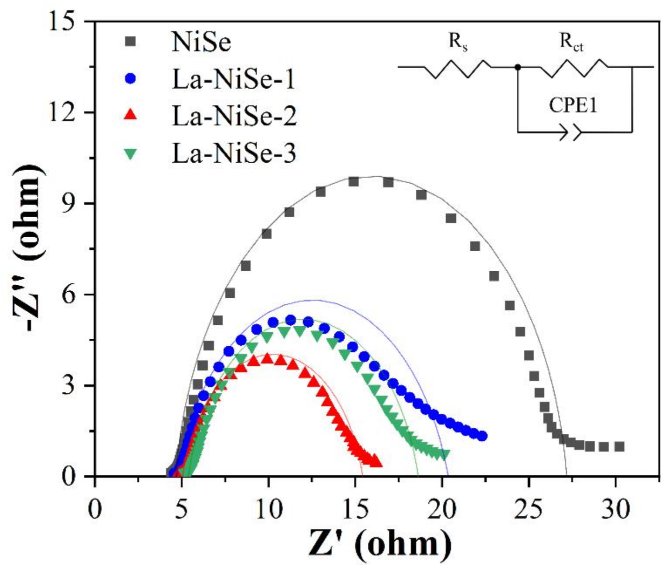

Figure S10. The EIS curves of the NiSe, La-NiSe-1, La-NiSe-2, La-NiSe-3 electrocatalysts in 1 M KOH with 0.33 M urea solution.

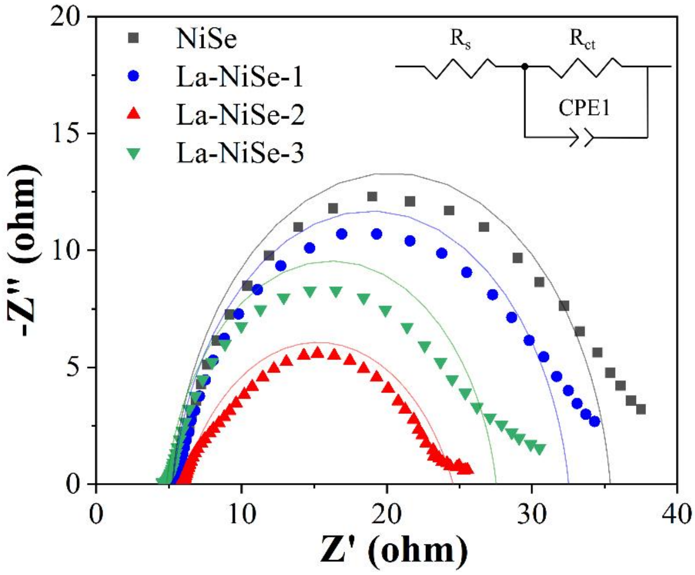

Figure S11. The EIS curves of the NiSe, La-NiSe-1, La-NiSe-2, La-NiSe-3 electrocatalysts in 1 M KOH.

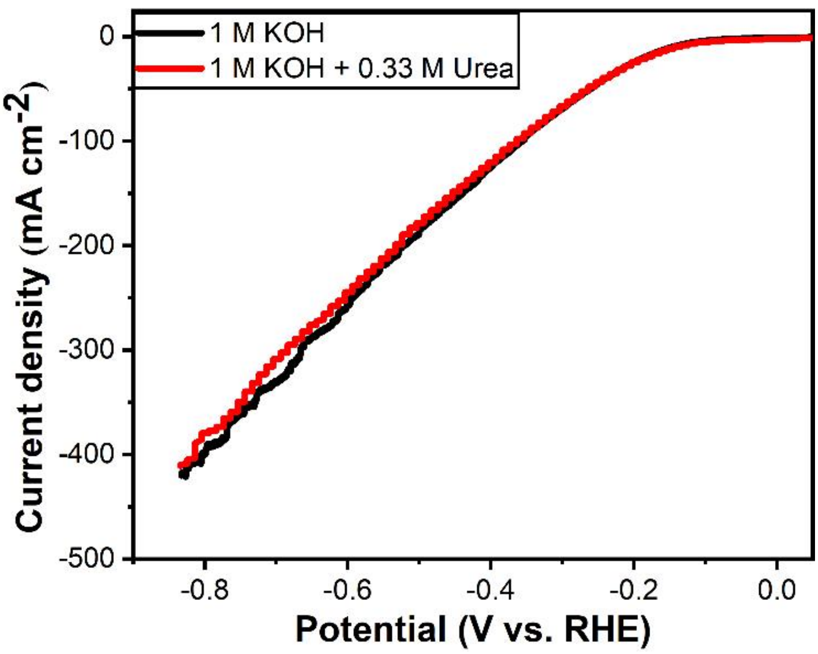

Figure S12. Comparison of LSV curves of La-NiSe-2 electrocatalysts collected in 1 M KOH with and without 0.33 M urea.

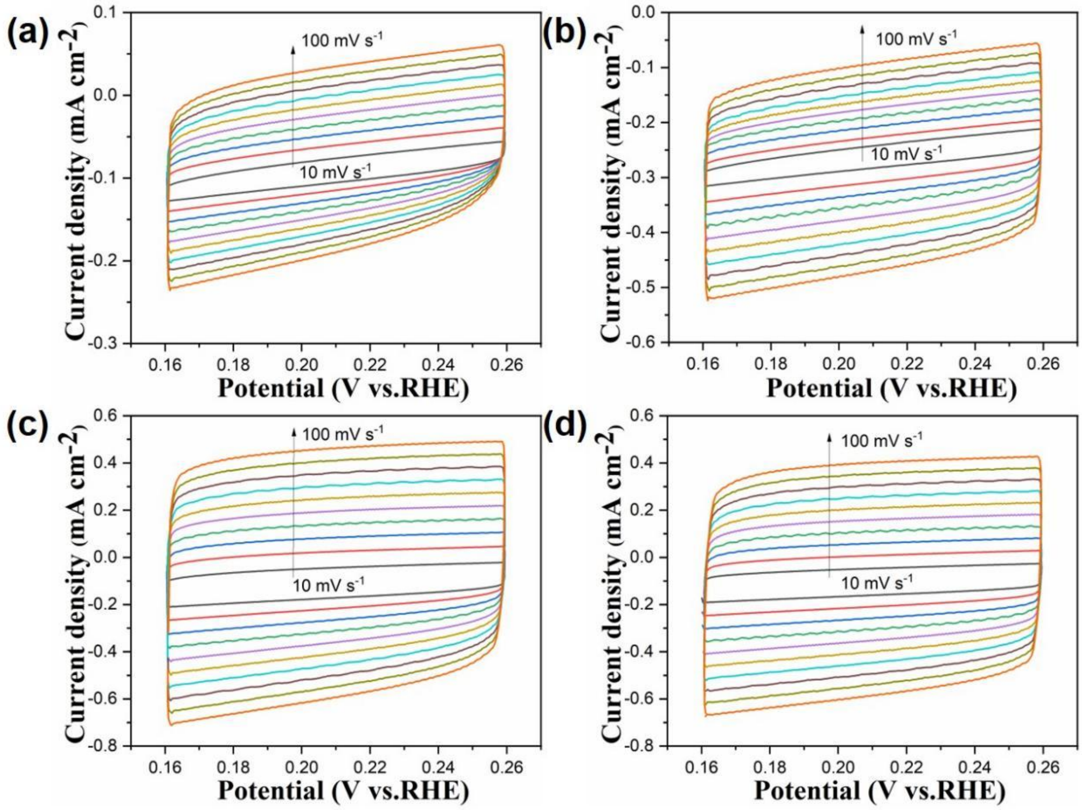

Figure S13. The CV curves of the (a) NiSe, (b) La-NiSe-1, (c) La-NiSe-2, (d) La-NiSe-3 electrocatalysts and corresponding (e) C_{dl} values in 1 M KOH solution.

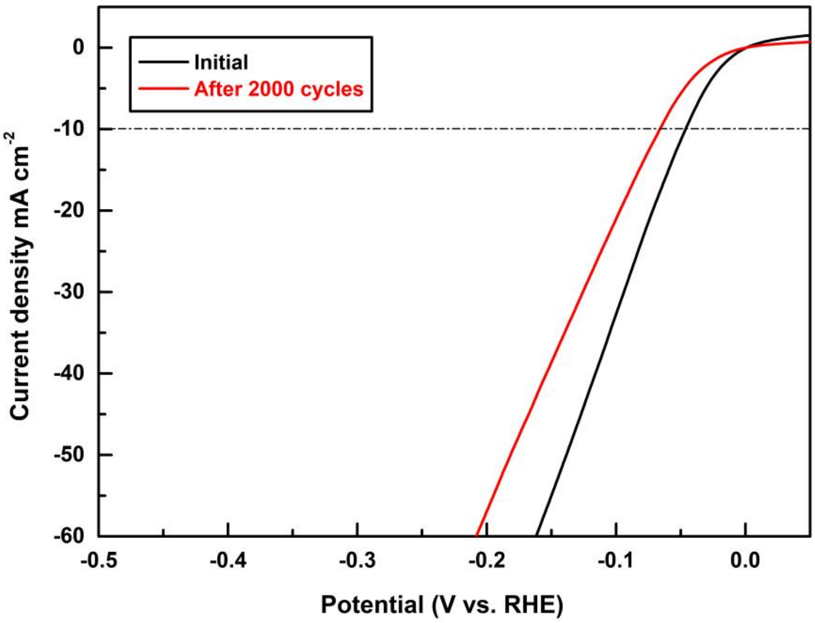

Figure S14. The LSV curves of the Pt/C electrocatalysts before and after 2000 cycles in 1 M KOH solution.

S4. Mechanism analysis.

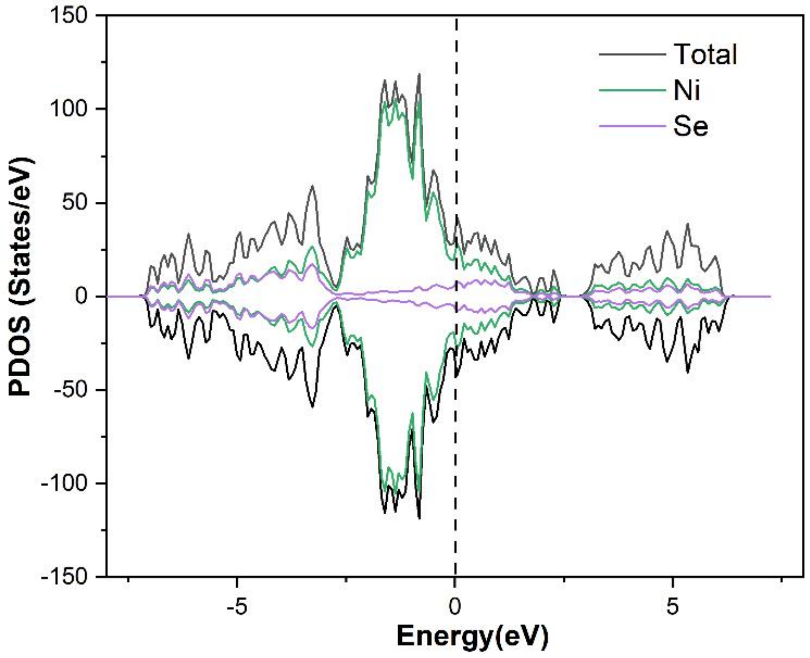

Figure S15. Projected Density of States (PDOS) of the NiSe system, with the Fermi level set to zero energy.

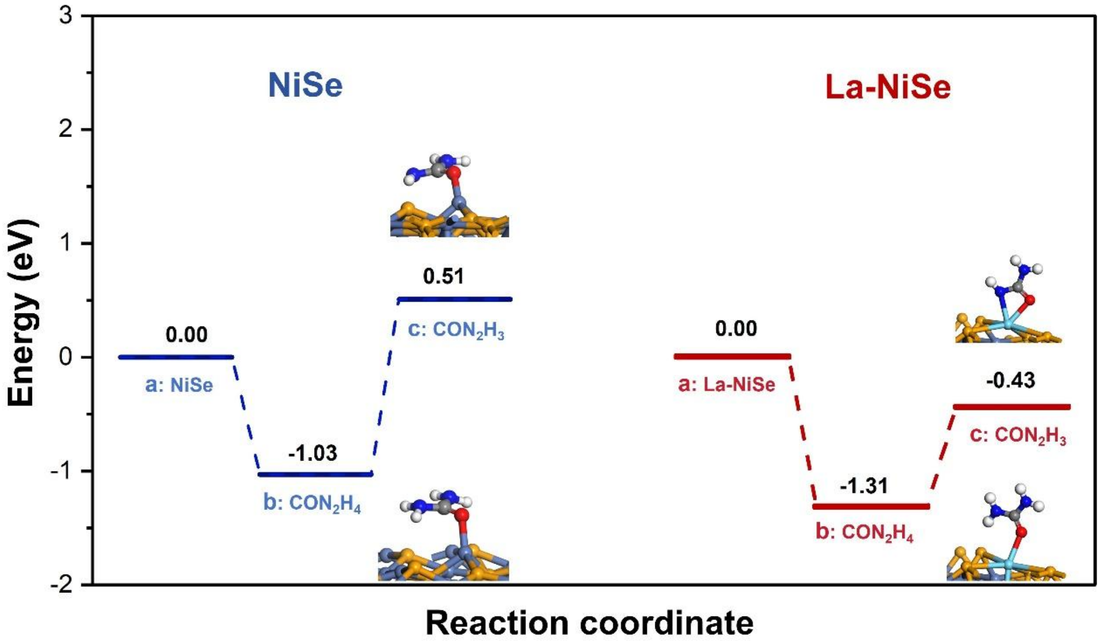

Figure S16. The key urea oxidation pathways and the corresponding energy profiles for NiSe and La-NiSe catalysts.

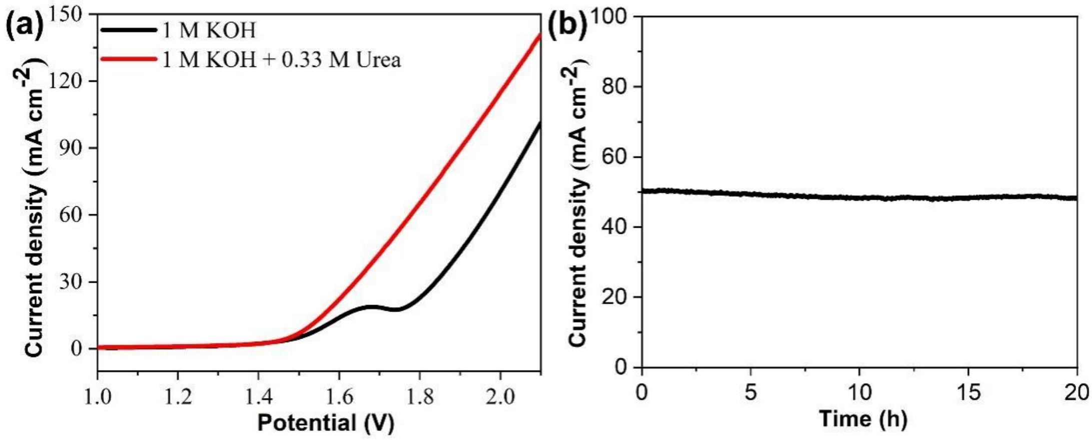

Figure S17. Comparison of LSV curves of the two-electrode setup of La-NiSe-2‖La-NiSe-2 in 1 M KOH with and without 0.33 M urea electrolyte. (b) Chronoamperometric stability test of urea-assisted water electrolysis employed La-NiSe-2‖La-NiSe-2 in 1 M KOH and 0.33 M urea.

Table S1. Comparison of UOR performances of La-NiSe-2 with other types methods of recently reported nickel selenide catalysts

Catalysts	Electrolyte	η_{10} (V) for UOR	Current density at 1.6 V vs. RHE (mA cm^{-2})	Tafel slope (mV dec^{-1})	Stability (h)	Ref
La-NiSe-2	1 M KOH + 0.33 M Urea	1.38	213	44.3	50	**This work**
$Ni_{0.85}Se$@CNTs-SS	1 M KOH + 0.33 M Urea	1.39	40	85	22	S7
NiSe@SM	1 M KOH + 0.33 M Urea	1.38	120	47	9	S8
NiMoSe/NF	1 M NaOH + 0.33 M Urea	1.4	175	43.3	10	S9
$FeSe_2$@Fe_2O_3/NiSe	1 M NaOH + 0.33 M Urea	1.38	210	57	12	S10
NiSe@MoS_2/NF	1 M KOH + 0.5 M Urea	1.42	/	30	30	S11
$Ni_{0.85}Se/NiSe_2$	1 M KOH + 0.33 M Urea	1.36	184	80.4	7	S12
Fe-$NiSe_2$–2	1 M KOH + 0.33 M Urea	1.38	120	22.9	2	S13
$NiSe_2$@$MoSe_2$	1 M KOH + 0.33 M Urea	1.36	120	41	2	S14
4NiAlSe-450	1 M KOH + 0.5 M Urea	1.36	110	/	3	S15
r-Se/$NiSe_2$/NF	1 M KOH + 0.33 M Urea	1.38	190	54	20	S16
$NiFeCoSe_2$	1 M KOH + 0.33 M Urea	1.37	150	149	30	S17

Table S2. EIS fitting parameters from equivalent circuits for different catalysts for UOR from Figure S10

Sample	R_s (Ω)	R_{ct} (Ω)	CPE1-T/S S^{-n}	CPE1-P/S S^{-n}
NiSe	4.65	22.52	5.81E-4	9.19E-1
La-NiSe-1	4.71	15.63	1.88E-3	8.15E-1
La-NiSe-2	5.04	10.38	1.79E-3	8.41E-1
La-NiSe-3	5.37	13.25	1.57E-3	8.46E-1

Table S3. EIS fitting parameters from equivalent circuits for different catalysts for OER from Figure S11

Sample	R_s (Ω)	R_{ct} (Ω)	CPE1-T/S S^{-n}	CPE1-P/S S^{-n}
NiSe	5.23	30.16	1.87E-3	9.21E-1
La-NiSe-1	5.27	27.25	1.93E-3	9.03E-1
La-NiSe-2	5.95	18.62	1.15E-3	7.35E-1
La-NiSe-3	4.83	22.71	1.71E-3	8.90E-1

Table S4. EIS fitting parameters from equivalent circuits for different catalysts for HER from Figure 4d

Sample	R_s (Ω)	R_{ct} (Ω)	CPE1-T/S S^{-n}	CPE1-P/S S^{-n}
NiSe	1.79	13.05	9.60E-6	9.44E-1
La-NiSe-1	1.90	8.06	1.27E-5	9.72E-1
La-NiSe-2	1.83	4.84	1.27E-5	9.68E-1
La-NiSe-3	1.72	5.61	2.20E-5	9.67E-1

References

[S1] Kresse, G.; Furthmüller, J. Efficient iterative schemes for ab initio total-energy calculations using a plane-wave basis set. *Phys. Rev. B* **1996**, *54*, 11169-11186.

[S2] Blöchl, P. E. Projector augmented-wave method. *Phys. Rev. B* **1994**, *50*, 17953-17979.

[S3] Kresse, G.; Joubert, D. From ultrasoft pseudopotentials to the projector augmented-wave method. *Phys. Rev. B* **1999**, *59*, 1758-1775.

[S4] Perdew, J. P.; Burke, K.; Ernzerhof, M. Generalized Gradient Approximation Made Simple. *Phys. Rev. Lett.* **1996**, *77*, 3865-3868.

[S5] Grimme, S.; Antony, J.; Ehrlich, S.; Krieg, H. A consistent and accurate ab initio parametrization of density functional dispersion correction (DFT-D) for the 94 elements H-Pu. *J. Chem. Phys.* **2010**, *132*, 154104.

[S6] Monkhorst, H. J.; Pack, J. D. Special points for Brillouin-zone integrations. *Phys. Rev. B* **1976**, *13*, 5188-5192.

[S7] Mathankumar, M.; Tu, S. L.; Hasin, P.; Hsieh, C. K.; Lin, J. Y. Efficient electrocatalytic nanocomposites of carbon nanotubes decorated with nickel selenides for urea oxidation reaction. *Int. J. Hydrogen Energy* **2024**, *77*, 373-382.

[S8] Ojha, S. K.; Kamlesh, Tiwari, S.; Mudgal, M.; Raizada, P.; Singh, P.; Singh, A.

Electrodeposited Ni-Se on recycled steel substrate as eco-friendly electrodes with enhanced electrocatalytic activity towards urea oxidation reaction. *J. Appl. Electrochem.* **2025**, *55*, 631-647.

[S9] Wang, H.; Jiao, X.; Zeng, W.; Zhang, Y.; Jiao, Y. Electrodeposition NiMoSe ternary nanoshperes on nickel foam as bifunctional electrocatalyst for urea electrolysis and hydrogen evolution reaction. *Int. J. Hydrogen Energy* **2021**, *46*, 37792-37801.

[S10] Desalegn, B. Z.; Hern, K.; Gil Seo, J. Synergistically interfaced bifunctional transition metal selenides for high-rate hydrogen production via urea electrolysis. *ChemCatChem* **2022**, *14*, e202100969.

[S11] Li, Y.; Bao, W.; Zhang, J.; Ai, T.; Wu, D.; Wang, H.; Yang, C.; Feng, L. Ultrathin MoS_2 nanosheets decorated on NiSe nanowire arrays as advanced trifunctional electrocatalyst for overall water splitting and urea electrolysis. *J. Ind. Eng. Chem.* **2023**, *121*, 510-518.

[S12] Cao, Q.; Huang, W.; Shou, J.; Sun, X.; Wang, K.; Zhao, Y.; Ding, R.; Lin, W.; Liu, E.; Gao, P. Coupling dual-phased nickel selenides with N-doped carbon enables efficient urea electrocatalytic oxidation. *J. Colloid Interf. Sci.* **2023**, *629*, 33-43.

[S13] Yu, L.; Pang, X.; Tian, Z.; Wang, S.; Feng, L. Fe-doped $NiSe_2$ nanorods for enhanced urea electrolysis of hydrogen generation. *Electrochim. Acta* **2023**, *440*, 141724.

[S14] Yin, C.; Yang, F.; Wang, S.; Feng, L. Heterostructured $NiSe_2$/$MoSe_2$ electronic modulation for efficient electrocatalysis in urea assisted water splitting reaction. *Chinese J. Catal.* **2023**, *51*, 225-236.

[S15] Wang, X.; Wang, J.; Xu, A.; Chang, Y.; Jia, J.; Jia, M. Effect of in situ growth of $NiSe_2$ on NiAl layered double hydroxide on its electrocatalytic properties for methanol and urea. *Int. J. Hydrogen Energy* **2023**, *48*, 22060-22068.

[S16] Khatun, S.; Roy, P. Mott-Schottky heterojunction of Se/$NiSe_2$ as bifunctional electrocatalyst for energy efficient hydrogen production via urea assisted seawater electrolysis. *J. Colloid Interf. Sci.* **2023**, *630*, 844-854.

[S17] Li, X.; Babar, P.; Patil, K.; Kale, S.; Jo, E.; Chen, X.; Hussain, Z.; Kim, J.H.; Yoo, Y.T. Bifunctional Ni-Fe-$CoSe_2$ nanosheets electrodeposited on Ni foam for efficient catalysis of the oxidation of water and urea. *Mater. Chem. Phys.* **2022**, *287*, 126310.